A Numerical Simulation for Darcy-Forchheimer Flow of Nanofluid by a Rotating Disk With Partial Slip Effects

Malik Zaka Ullah [1]*, Stefano Serra-Capizzano [2,3] and Dumitru Baleanu [4,5]

[1] *Department of Mathematics, Faculty of Science, King Abdulaziz University, Jeddah, Saudi Arabia, [2] Department of Science and High Technology, University of Insubria, Como, Italy, [3] Department of Information Technology, Uppsala University, Uppsala, Sweden, [4] Department of Mathematics, Cankaya University, Ankara, Turkey, [5] Institute of Space Sciences, Bucharest, Romania*

This study examines Darcy-Forchheimer 3D nanoliquid flow caused by a rotating disk with heat generation/absorption. The impacts of Brownian motion and thermophoretic are considered. Velocity, concentration, and thermal slips at the surface of the rotating disk are considered. The change from the non-linear partial differential framework to the non-linear ordinary differential framework is accomplished by utilizing appropriate variables. A shooting technique is utilized to develop a numerical solution of the resulting framework. Graphs have been sketched to examine how the concentration and temperature fields are affected by several pertinent flow parameters. Skin friction and local Sherwood and Nusselt numbers are additionally plotted and analyzed. Furthermore, the concentration and temperature fields are enhanced for larger values of the thermophoresis parameter.

Keywords: rotating disk, Darcy-Forchheimer flow, nanoparticles, heat absorption/generation, slip conditions, numerical solution

1. INTRODUCTION

Flow due to a rotating disk plays an indispensable role in numerous modern items encompassing rotating machinery, apparatuses, rotors, and flywheels. As of late, rotating disks have become a significant component of many pieces of machinery, for example, thermal power-creation frameworks, rotor-stator turning circle reactors, electrical controls, stopping mechanisms, pivoting sawing machines, and rotational air cleaning systems. Close investigations of laminar boundary layer flow were carried out by Von Karman [1]. Turkyilmazoglu and Senel [2] examined the linked features of heat and mass exchange arising from the revolution of a hard and permeable disk. Entropy generation in slip flow by the turning of a permeable disk with MHD and variable properties was clarified by Rashidi et al. [3]. Nanofluid flow because of the revolution of a disk was explored by Turkyilmazoglu [4]. Hatami et al. [5] investigated the impacts of the contraction, turning, and heat of disks on the movement of nanofluids. They utilized a least-square strategy for solution development. Mustafa et al. [6] deciphered the three-dimensional rotating flow of nanofluids over a stationary disk. Sheikholeslami et al. [7] created numerical models of nanofluid splashing on a slanted turning disk. Transient thermophoretic molecule deposition through the constrained convective flow of micropolar liquid over a pivoting disk was examined by Doh and Muthtamilselvan [8]. Hayat et al. [9] discussed Darcy-Forchheimer flow of carbon nanotubes in

response to a turning disk. Aziz et al. [10] gave a numerical report on nanofluid flow from the pivoting of a disk, looking at the impacts of slip and heat absorption/generation. Synthetically responsive flow of third-grade nanofluid over a stretchable turning disk with heat generation was broken down by Hayat et al. [11]. The radiative flow of a suspension of nanoparticles and gyrotactic microorganisms by the variably thick surface of a turning disk was clarified by Qayyum et al. [12]. Hayat et al. [13] presented a numerical simulation of the radiative flow of carbon nanotubes due to the revolution of a disk with partial slip.

The low thermal productivity of working fluids is a guideline problem for several heat transport components in engineering applications. For this reason, some researchers are making efforts to develop an innovative course for the improvement of the thermal efficiency of working fluids. Various measures have been proposed by experts to improve the thermal efficiency of fluids. Accordingly, the incorporation of nanomaterial into the working fluid, making what is termed a nanofluid, is extremely promising. Recent assessments of nanofluids reveal that working fluid has totally different features with the addition of nanomaterial. This is because the thermal efficiency of the working liquid is lower than that of the nanomaterial. Nanofluid is suspension of fluids containing standard fluid with the particles of nano-measure. Such nanomaterials are utilized in materials, MHD control generators, oil stores, cooling of nuclear reactors, vehicle transformers, and various others [14–18]. Choi and Eastman [19] coined the term nanofluid. They proposed that nanomaterials are a groundbreaking contender for the development of heat transport via the customary fluids. Buongiorno proposed a numerical model of convective transport by nanofluid [20]. Here, thermophoresis and Brownian motion are viewed as the most important slip mechanisms. Heat transfer increase by nanofluids in a two-sided top-driven heated square hole was considered by Tiwari and Das [21]. The significance of a CuO-water nanomaterial on the outside of heat exchangers was tentatively examined by Pantzali et al. [22]. Few ongoing studies on nanofluid flow can be found in the literature [23–45].

Motivated by the above-mentioned articles, the objective here is to examine the impacts of heat absorption/generation in Darcy-Forchheimer 3D nanofluid flow caused by a rotating disk and the impacts of slip. Both Brownian diffusion and thermophoretic phenomena occur in view of the existence of nanoparticles. Velocity, concentration, and thermal slips are accounted for. The obtained framework is solved numerically by the shooting technique. Concentration, temperature, skin friction, and local Sherwood and Nusselt numbers are also analyzed through plots.

2. MATHEMATICAL MODELING

Let us examine steady Darcy-Forchheimer 3D nanoliquid flow caused by a rotating disk with slip and heat absorption/generation. A disk at $z = 0$ rotates with constant

FIGURE 1 | Flow model and coordinate system.
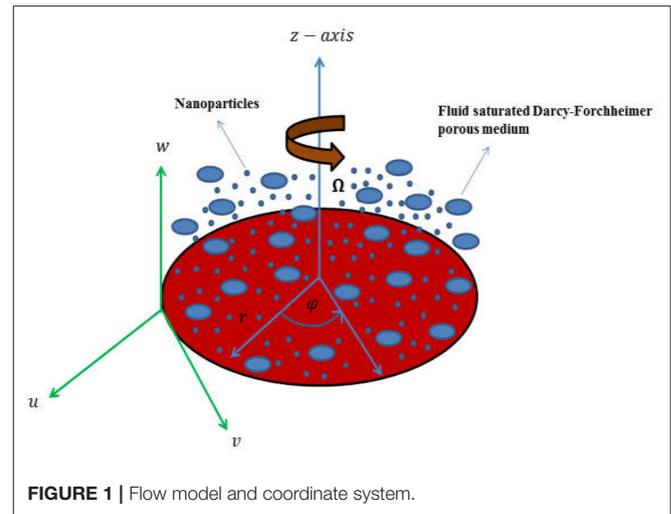
angular velocity Ω (see **Figure 1**). The impacts of Brownian motion and thermophoretis are accounted for. The velocities are (u, v, w) in the directions of increase in (r, φ, z), respectively. The resulting boundary layer expressions are [45, 46]:

$$\frac{\partial u}{\partial r} + \frac{u}{r} + \frac{\partial w}{\partial z} = 0, \tag{1}$$

$$u\frac{\partial u}{\partial r} - \frac{v^2}{r} + w\frac{\partial u}{\partial z} = v\left(\frac{\partial^2 u}{\partial z^2} + \frac{\partial^2 u}{\partial r^2} + \frac{1}{r}\frac{\partial u}{\partial r} - \frac{u}{r^2}\right) - \frac{v}{k^*}u - Fu^2, \tag{2}$$

$$u\frac{\partial v}{\partial r} + \frac{uv}{r} + w\frac{\partial v}{\partial z} = v\left(\frac{\partial^2 v}{\partial z^2} + \frac{\partial^2 v}{\partial r^2} + \frac{1}{r}\frac{\partial v}{\partial r} - \frac{v}{r^2}\right) - \frac{v}{k^*}v - Fv^2, \tag{3}$$

$$u\frac{\partial w}{\partial r} + w\frac{\partial w}{\partial z} = v\left(\frac{\partial^2 w}{\partial z^2} + \frac{\partial^2 w}{\partial r^2} + \frac{1}{r}\frac{\partial w}{\partial r}\right) - \frac{v}{k^*}w - Fw^2, \tag{4}$$

$$\begin{aligned}
u\frac{\partial T}{\partial r} + w\frac{\partial T}{\partial z} &= \alpha^*\left(\frac{\partial^2 T}{\partial z^2} + \frac{\partial^2 T}{\partial r^2} + \frac{1}{r}\frac{\partial T}{\partial r}\right) + \frac{Q}{(\rho c)_f}(T - T_\infty) \\
&+ \frac{(\rho c)_p}{(\rho c)_f}\left(D_B\left(\frac{\partial T}{\partial r}\frac{\partial C}{\partial r} + \frac{\partial T}{\partial z}\frac{\partial C}{\partial z}\right)\right. \\
&+ \left.\frac{D_T}{T_\infty}\left(\left(\frac{\partial T}{\partial z}\right)^2 + \left(\frac{\partial T}{\partial r}\right)^2\right)\right),
\end{aligned} \tag{5}$$

$$\begin{aligned}
u\frac{\partial C}{\partial r} + w\frac{\partial C}{\partial z} &= D_B\left(\frac{\partial^2 C}{\partial z^2} + \frac{\partial^2 C}{\partial r^2} + \frac{1}{r}\frac{\partial C}{\partial r}\right) \\
&+ \frac{D_T}{T_\infty}\left(\frac{\partial^2 T}{\partial z^2} + \frac{\partial^2 T}{\partial r^2} + \frac{1}{r}\frac{\partial T}{\partial r}\right).
\end{aligned} \tag{6}$$

It is subject to the boundary conditions [10] :

$$u = L_1\frac{\partial u}{\partial z}, \ v = r\Omega + L_1\frac{\partial v}{\partial z}, \ w = 0, \ T = T_w + L_2\frac{\partial T}{\partial z},$$

$$C = C_w + L_3 \frac{\partial C}{\partial z} \quad \text{at } z = 0, \tag{7}$$

$$u \to 0, \quad v \to 0, \quad T \to T_\infty, \quad C \to C_\infty \quad \text{as } z \to \infty. \tag{8}$$

Here u, v, and w represent the velocity components in the directions r, φ, and z while ρ_f, μ and, $v (= \mu/\rho_f)$ depict the fluid density, dynamic, and kinematic viscosities respectively, C_b the drag factor, L_1 the velocity slip factor, L_2 the thermal slip factor $(\rho c)_p$, the effective heat capacity of nanoparticles, T the fluid temperature, k^* the permeability of porous space, C the concentration $(\rho c)_f$, the heat capacity of the liquid, L_3 the concentration slip factor, C_∞ the ambient concentration, D_T the thermophoretic factor, $F = C_b/rk^{*1/2}$ the non-uniform inertia factor, k and $\alpha^* = k/(\rho c)_f$ the thermal conductivity and thermal diffusivity, respectively, D_B the Brownian factor, Q the heat generation/absorption factor and T_∞ the ambient temperature. Selecting [10]:
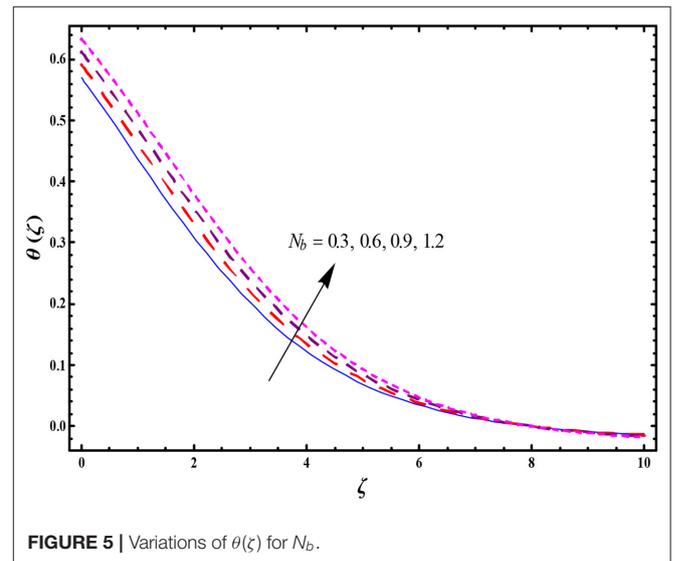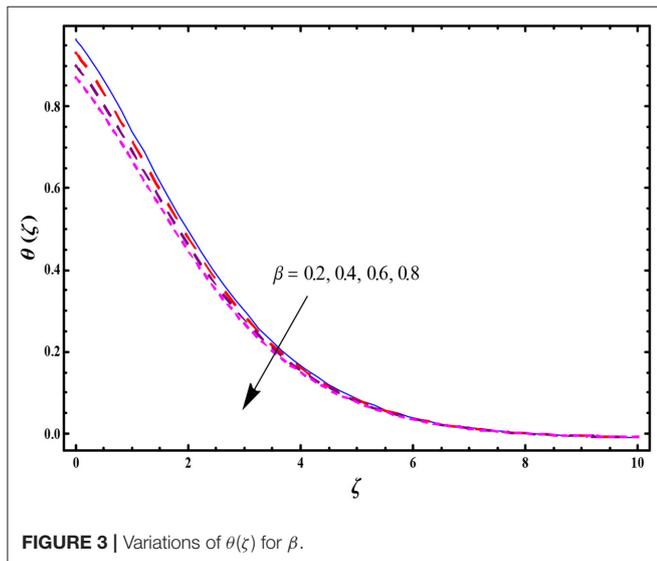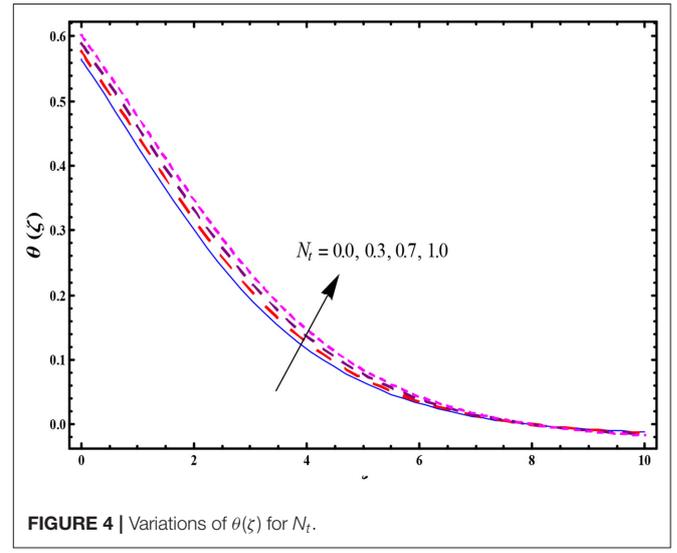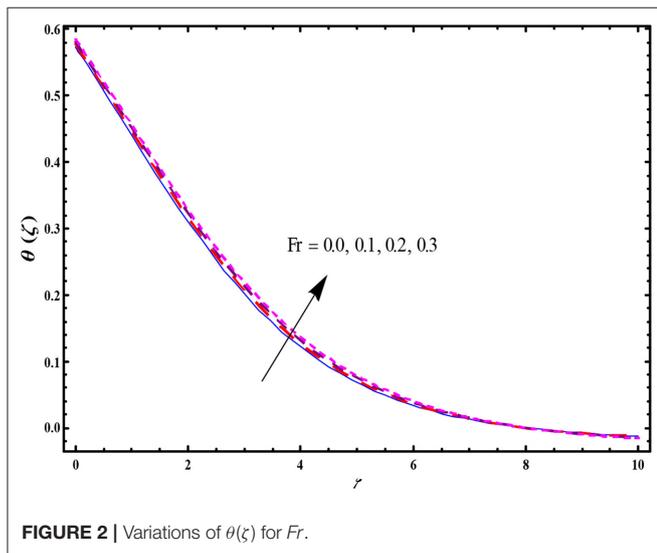
$$\left. \begin{array}{l} u = r\Omega f'(\zeta), \quad w = -(2\Omega v)^{1/2} f(\zeta), \quad v = r\Omega g(\zeta), \\ \phi(\zeta) = \frac{C - C_\infty}{C_w - C_\infty}, \quad \zeta = \left(\frac{2\Omega}{v}\right)^{1/2} z, \quad \theta(\zeta) = \frac{T - T_\infty}{T_w - T_\infty}. \end{array} \right\} \tag{9}$$

Continuity Equation (1) is trivially verified, while Equations (2)− (8) yield

$$2f''' + 2ff'' - f'^2 + g^2 - \lambda f' - Frf'^2 = 0, \tag{10}$$

$$2g'' + 2fg' - 2f'g - \lambda g - Frg^2 = 0, \tag{11}$$

$$\frac{1}{Pr}\theta'' + f\theta' + N_b\theta'\phi' + N_t\theta'^2 + \delta\theta = 0, \tag{12}$$

FIGURE 2 | Variations of $\theta(\zeta)$ for Fr.

FIGURE 4 | Variations of $\theta(\zeta)$ for N_t.

FIGURE 3 | Variations of $\theta(\zeta)$ for β.

FIGURE 5 | Variations of $\theta(\zeta)$ for N_b.

$$\frac{1}{Sc}\phi'' + f\phi' + \frac{1}{Sc}\frac{N_t}{N_b}\theta'' = 0, \tag{13}$$
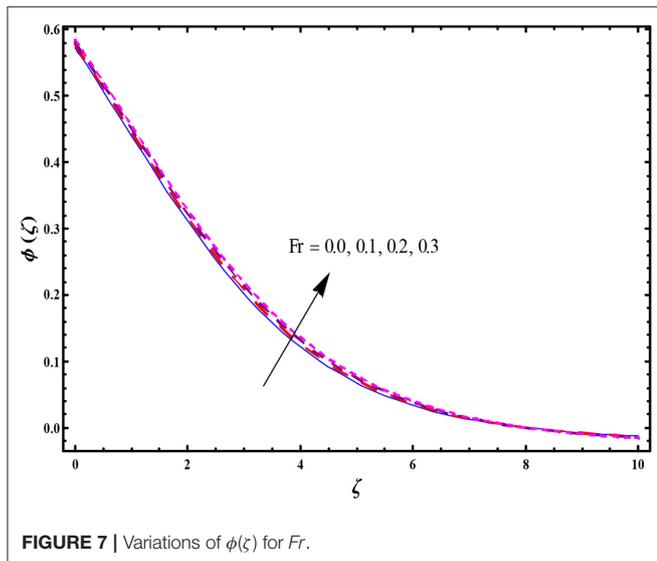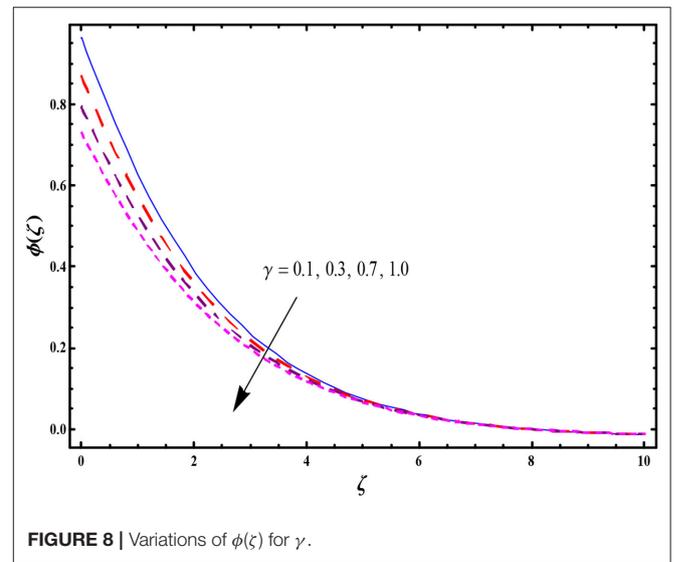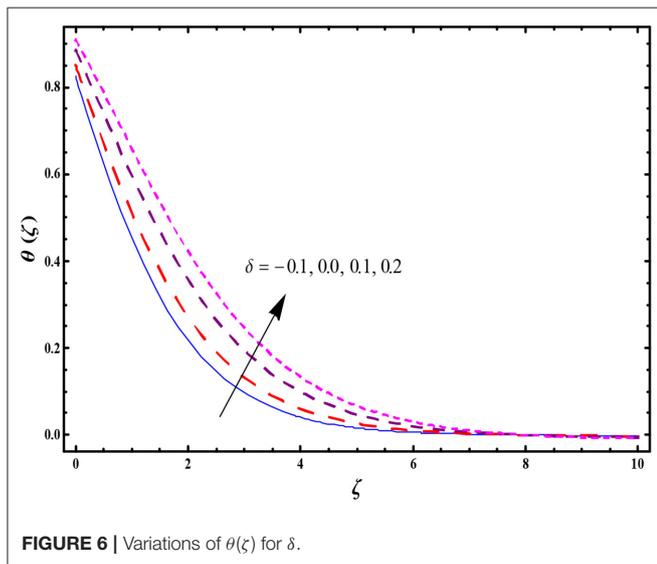
$$f(0) = 0, \ f'(0) = \alpha f''(0), \ g(0) = 1 + \alpha g'(0),$$
$$\theta(0) = 1 + \beta\theta'(0), \ \phi(0) = 1 + \gamma\phi'(0), \tag{14}$$

$$f'(\infty) \to 0, \ g(\infty) \to 0, \ \theta(\infty) \to 0, \ \phi(\infty) \to 0. \tag{15}$$

Here, Fr stands for the Forchheimer number, α for the velocity slip parameter, λ for the porosity parameter, N_t for the thermophoresis parameter, β for the thermal slip parameter, Pr for the Prandtl number, N_b for Brownian motion, δ for the heat absorption/generation parameter, γ for the concentration slip parameter, and Sc for the Schmidt number. Non-dimensional variables are defined by

$$\left.\begin{array}{c} \lambda = \frac{\nu}{k^*\Omega}, \ \alpha = L_1\sqrt{\frac{2\Omega}{\nu}}, \ Fr = \frac{C_b}{k^{*1/2}}, \ N_b = \frac{(\rho c)_p D_B (C_w - C_\infty)}{(\rho c)_f \nu}, \\[2mm] \delta = \frac{Q}{2\Omega(\rho c)_f}, \\[2mm] \beta = L_2\sqrt{\frac{2\Omega}{\nu}}, \ \mathrm{Pr} = \frac{\nu}{\alpha^*}, \ N_t = \frac{(\rho c)_p D_T (T_w - T_\infty)}{(\rho c)_f \nu T_\infty}, \ \gamma = L_3\sqrt{\frac{2\Omega}{\nu}}, \\[2mm] Sc = \frac{\nu}{D_B}. \end{array}\right\} \tag{16}$$

FIGURE 6 | Variations of $\theta(\zeta)$ for δ.

FIGURE 8 | Variations of $\phi(\zeta)$ for γ.

FIGURE 7 | Variations of $\phi(\zeta)$ for Fr.

FIGURE 9 | Variations of $\phi(\zeta)$ for N_t.
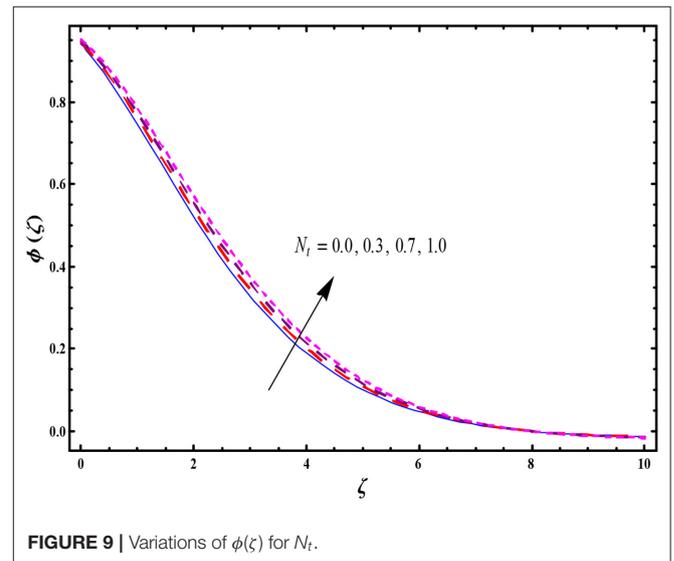
The coefficients of skin friction and the Nusselt and Sherwood numbers are

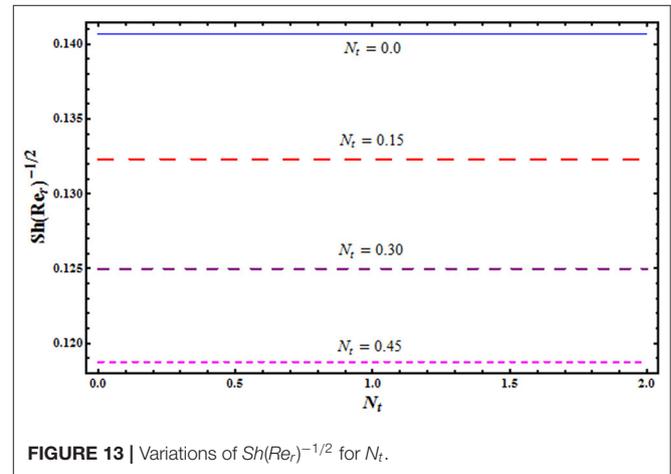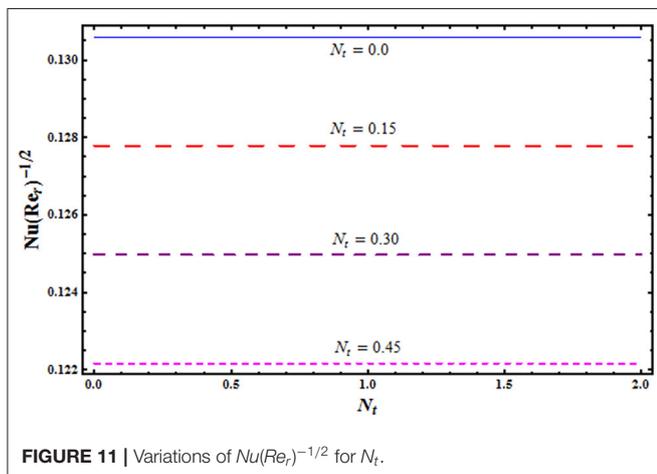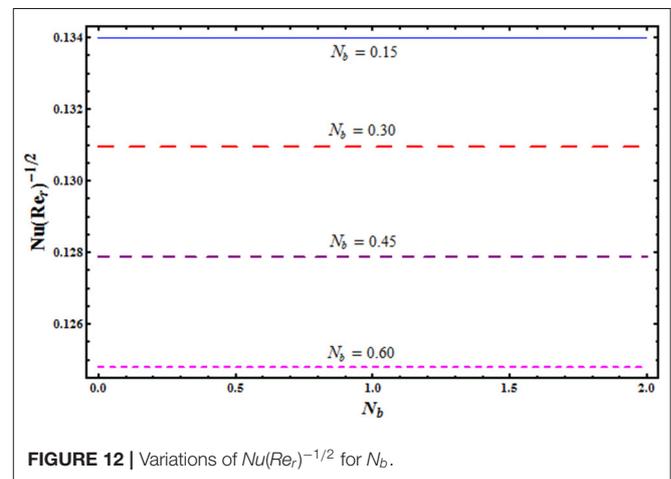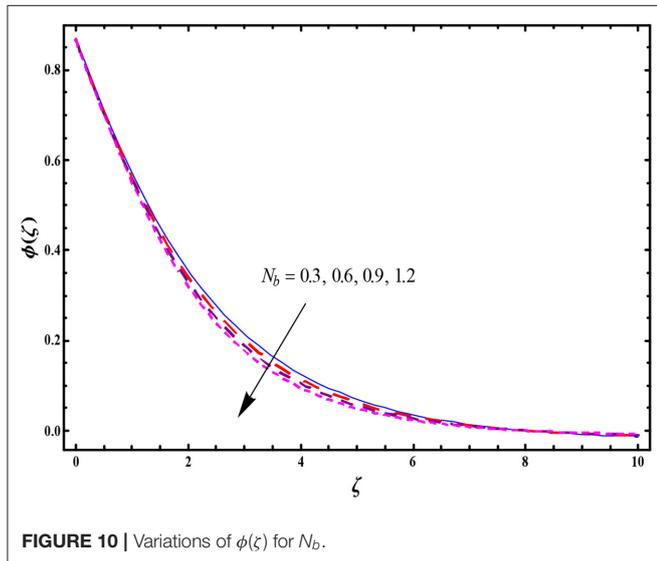$$Re_r^{1/2}C_f = f''(0), \ Re_r^{1/2}C_g = g'(0), \ Re_r^{-1/2}Nu = -\theta'(0),$$
$$Re_r^{-1/2}Sh = -\phi'(0), \tag{17}$$

where $Re_r = 2(\Omega r)r/\nu$ represents the local rotational Reynolds number.

3. NUMERICAL RESULTS AND DISCUSSION

This section depicts the contributions of various physical variables like thermophoresis parameter N_t, Forchheimer number Fr, thermal slip parameter β, heat generation/absorption parameter δ, Brownian number N_b, and concentration slip number γ on The concentration $\phi(\zeta)$ and temperature $\theta(\zeta)$ distributions. The effect of Forchheimer variable Fr

on $\theta(\zeta)$ is portrayed in **Figure 2**. A larger value for Fr shows expanding behavior of $\theta(\zeta)$ and the related thermal layer. **Figure 3** shows the impact of thermal slip β on temperature $\theta(\zeta)$. Temperature is reduced by increasing thermal slip β. **Figure 4** demonstrates the effect of N_t on the temperature field $\theta(\zeta)$. A larger thermophoresis parameter N_t value leads to a higher temperature field and thicker dynamically warm layer. The reason for this conflict is that growth in N_t yields high grounded thermophoresis control, which further allows movement of the nanoparticles in the fluid zone. A long way from the surface, a more grounded temperature scattering $\theta(\zeta)$ and continuously warm layer is thus created. The impact of N_b on the temperature profile $\theta(\zeta)$ is portrayed in **Figure 5**. Physically, the irregularity of nanoparticle movement increases by enhancing Brownian motion, due to which collision of particles occurs. Thus, kinetic energy is converted into heat energy, which produces an increase in the temperature field. **Figure 6** shows how heat generation/absorption δ influences
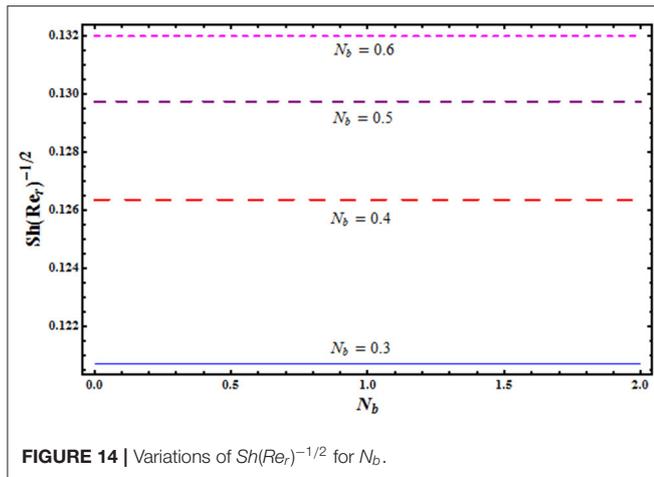

FIGURE 10 | Variations of $\phi(\zeta)$ for N_b.

FIGURE 12 | Variations of $Nu(Re_r)^{-1/2}$ for N_b.

FIGURE 11 | Variations of $Nu(Re_r)^{-1/2}$ for N_t.

FIGURE 13 | Variations of $Sh(Re_r)^{-1/2}$ for N_t.

FIGURE 14 | Variations of $Sh(Re_r)^{-1/2}$ for N_b.

TABLE 1 | Comparative values of $f''(0)$ and $g'(0)$ for value of Fr when $\lambda = 0.2$ and $\alpha = 0$.

	Present results		Naqvi et al. [45]	
Fr	$f''(0)$	$g'(0)$	$f''(0)$	$g'(0)$
0.2	0.43478	-0.78139	0.4347813	-0.7813904

temperature dispersion $\theta(\zeta)$. Here, $\delta > 0$ portrays heat generation and $\delta < 0$ for heat absorption. Both temperature $\theta(\zeta)$ and the warm layer are upgraded with increasing δ. **Figure 7** shows that concentration $\phi(\zeta)$ is higher for larger values of the Forchheimer variable Fr. **Figure 8** shows how concentration $\phi(\zeta)$ is influenced by concentration slip γ. Concentration is reduced at higher estimations of γ. **Figure 9** demonstrates how the thermophoresis parameter N_t influences the concentration $\phi(\zeta)$. By improving thermophoresis parameter N_t, the concentration $\phi(\zeta)$ is increased. **Figure 10** depicts the impact of Brownian motion N_b on concentration $\phi(\zeta)$. It has been noted that a stronger concentration $\phi(\zeta)$ is developed by utilizing greater N_b. **Figures S1**, **S2** display the impacts of Fr on $C_f Re_r^{1/2}$ and $C_g Re_r^{1/2}$, respectively. It is noted that $C_f Re_r^{1/2}$ is a decaying function of Fr, while the reverse situation is observed for $C_g Re_r^{1/2}$. The effects of N_t and N_b on $Nu(Re_r)^{-1/2}$ are highlighted in **Figures 11**, **12**, respectively. Here, $Nu(Re_r)^{-1/2}$ reduces for N_t and N_b. The effects of N_t and N_b on $Sh(Re_r)^{-1/2}$ are portrayed in **Figures 13**, **14**, respectively. Here,

$Sh(Re_r)^{-1/2}$ is an increasing factor of N_t, while the opposite trend is seen for N_b. The figures in **Table 1** were computed to validate the present results with previously published results in a limiting sense. Here, we see that the present numerical solution is in good agreement with the previous solution by Naqvi et al. [45] in a limiting sense.

4. CONCLUSIONS

In this paper, Darcy-Forchheimer 3D nanofluid flow caused by a rotating disk with heat generation/absorption is studied. Brownian motion and thermophoretic phenomena occur with the existence of nanoparticles. Velocity, concentration, and thermal slips are accounted for. A higher Forchheimer number Fr depicts similar behavior for concentration and temperature. A larger β corresponds to a lower temperature field. Higher γ depicts decreasing behavior for the concentration field. A stronger temperature field is observed for N_b and N_t. Concentration $\phi(\zeta)$ displays the reverse behavior for N_b and N_t.

DATA AVAILABILITY STATEMENT

The datasets generated for this study are available on request to the corresponding author.

AUTHOR CONTRIBUTIONS

All authors listed have made a substantial, direct and intellectual contribution to the work, and approved it for publication.

ACKNOWLEDGMENTS

SUPPLEMENTARY MATERIAL

The Supplementary Material for this article can be found online at: https://www.frontiersin.org/articles/10.3389/fphy.2019.00219/full#supplementary-material

Figure S1 | Variations of $C_f Re_r^{1/2}$ for Fr.

Figure S2 | Variations of $CgRe_r^{1/2}$ for Fr.

REFERENCES

1. Von Karman T. Uber laminare and turbulente Reibung. *Z Angew Math Mech*. (1921) **1**:233–52. doi: 10.1002/zamm.19210010401

2. Turkyilmazoglu M, Senel P. Heat and mass transfer of the flow due to a rotating rough and porous disk. *Int J Therm Sci*. (2013) **63**:146–58. doi: 10.1016/j.ijthermalsci.2012.07.013

3. Rashidi MM, Kavyani N, Abelman S. Investigation of entropy generation in MHD and slip flow over rotating porous disk with

variable properties. *Int J Heat Mass Transf*. (2014) **70**:892–917. doi: 10.1016/j.ijheatmasstransfer.2013.11.058

4. Turkyilmazoglu M. Nanofluid flow and heat transfer due to a rotating disk. *Comput Fluids*. (2014) **94**:139–46. doi: 10.1016/j.compfluid.2014.02.009

5. Hatami M, Sheikholeslami M, Gangi DD. Laminar flow and heat transfer of nanofluids between contracting and rotating disks by least square method. *Powder Technol*. (2014) **253**:769–79. doi: 10.1016/j.powtec.2013.12.053

6. Mustafa M, Khan JA, Hayat T, Alsaedi A. On Bödewadt flow and heat transfer of nanofluids over a stretching stationary disk. *J Mol Liquid*. (2015) **211**:119–25. doi: 10.1016/j.molliq.2015.06.065

7. Sheikholeslami M, Hatami M, Ganji DD. Numerical investigation of nanofluid spraying on an inclined rotating disk for cooling process. *J Mol Liquid.* (2015) **211**:577–83. doi: 10.1016/j.molliq.2015.07.006

8. Doh DH, Muthtamilselvan M. Thermophoretic particle deposition on magnetohydrodynamic flow of micropolar fluid due to a rotating disk. *Int J Mech Sci.* (2017) **130**:350–9. doi: 10.1016/j.ijmecsci.2017.06.029

9. Hayat T, Haider F, Muhammad T, Alsaedi A. On Darcy-Forchheimer flow of carbon nanotubes due to a rotating disk. *Int J Heat Mass Transf.* (2017) **112**:248–54. doi: 10.1016/j.ijheatmasstransfer.2017.04.123

10. Aziz A, Alsaedi A, Muhammad T, Hayat T. Numerical study for heat generation/absorption in flow of nanofluid by a rotating disk. *Results Phys.* (2018) **8**:785–92. doi: 10.1016/j.rinp.2018.01.009

11. Hayat T, Ahmad S, Khan MI, Alsaedi A. Modeling and analyzing flow of third grade nanofluid due to rotating stretchable disk with chemical reaction and heat source. *Phys B.* (2018) **537**:116–26. doi: 10.1016/j.physb.2018.01.052

12. Qayyum S, Imtiaz M, Alsaedi A, Hayat T. Analysis of radiation in a suspension of nanoparticles and gyrotactic microorganism for rotating disk of variable thickness. *Chin J Phys.* (2018) **56**:2404–23. doi: 10.1016/j.cjph.2018.06.020

13. Hayat T, Khalid H, Waqas M, Alsaedi A. Numerical simulation for radiative flow of nanoliquid by rotating disk with carbon nanotubes and partial slip. *Comput Methods Appl Mech Eng.* (2018) **341**:397–408. doi: 10.1016/j.cma.2018.06.018

14. Mabood F, Ibrahim SM, Lorenzini G. Chemical reaction effects on MHD rotating fluid over a vertical plate embedded in porous medium with heat source. *J Eng Thermophys.* (2017) **26**:399–415. doi: 10.1134/S1810232817030109

15. Mabood F, Lorenzini G, Pochai N, Shateyi S. Homotopy analysis method for radiation and hydrodynamic-thermal slips effects on MHD flow and heat transfer impinging on stretching sheet. *Defect Diffusion Forum.* (2018) **388**:317–27. doi: 10.4028/www.scientific.net/DDF.388.317

16. Mabood F, Das K. Outlining the impact of melting on MHD Casson fluid flow past a stretching sheet in a porous medium with radiation. *Heliyon.* (2019) **5**:e01216. doi: 10.1016/j.heliyon.2019.e01216

17. Mabood F, Nayak MK, Chamkha AJ. Heat transfer on the cross flow of micropolar fluids over a thin needle moving in a parallel stream influenced by binary chemical reaction and Arrhenius activation energy. *Eur Phys J Plus.* (2019) **134**:427. doi: 10.1140/epjp/i2019-12716-9

18. Imtiaz M, Mabood F, Hayat T, Alsaedi A. Homogeneous-heterogeneous reactions in MHD radiative flow of second grade fluid due to a curved stretching surface. *Int J Heat Mass Transf.* (2019) **145**:118781. doi: 10.1016/j.ijheatmasstransfer.2019.118781

19. Choi SUS, Eastman JA. Enhancing thermal conductivity of fluids with nanoparticles. *ASME Int Mech Eng Cong Exp.* (1995) **66**:99–105.

20. Buongiorno J. Convective transport in nanofluids. *ASME J Heat Transf.* (2006) **128**:240–50. doi: 10.1115/1.2150834

21. Tiwari RK, Das MK. Heat transfer augmentation in a two-sided lid-driven differentially heated square cavity utilizing nanofluid. *Int J Heat Mass Transf.* (2007) **50**:2002–18. doi: 10.1016/j.ijheatmasstransfer.2006.09.034

22. Pantzali MN, Mouza AA, Paras SV. Investigating the efficacy of nanofluids as coolants in plate heat exchangers (PHE). *Chem Eng Sci.* (2009) **64**:3290–300. doi: 10.1016/j.ces.2009.04.004

23. Sheikholeslami M, Bandpy MG, Ganji DD, Soleimani S. Effect of a magnetic field on natural convection in an inclined half-anulus enclosure filled with Cu-water nanofluid using CVFEM. *Adv Powder Technol.* (2013) **24**:980–91. doi: 10.1016/j.apt.2013.01.012

24. Togun H, Safaei MR, Sadri R, Kazi SN, Badarudin A, Hooman K, et al. Numerical simulation of laminar to turbulent nanofluid flow and heat transfer over a backward-facing step. *Appl Math Comput.* (2014) **239**:153–70. doi: 10.1016/j.amc.2014.04.051

25. Hayat T, Aziz A, Muhammad T, Ahmad B. Influence of magnetic field in three-dimensional flow of couple stress nanofluid over a nonlinearly stretching surface with convective condition. *PLoS ONE.* (2015) **10**:e0145332. doi: 10.1371/journal.pone.0145332

26. Lin Y, Zheng L, Zhang X, Ma L, Chen G. MHD pseudo-plastic nanofluid unsteady flow and heat transfer in a finite thin film over stretching surface with internal heat generation. *Int J Heat Mass Transf.* (2015) **84**:903–11. doi: 10.1016/j.ijheatmasstransfer.2015.01.099

27. Hayat T, Muhammad T, Alsaedi A, Alhuthali MS. Magnetohydrodynamic three-dimensional flow of viscoelastic nanofluid in the presence of nonlinear thermal radiation. *J Magn Mater.* (2015) **385**: 222–9. doi: 10.1016/j.jmmm.2015.02.046

28. Gireesha BJ, Mahanthesh B, Shivakumara IS Eshwarappa KM. Melting heat transfer in boundary layer stagnation-point flow of nanofluid toward a stretching sheet with induced magnetic field. *Int J Eng Sci Technol.* (2016) **19**:313–21. doi: 10.1016/j.jestch.2015.07.012

29. Hayat T, Aziz A, Muhammad T, Alsaedi A. On magnetohydrodynamic three-dimensional flow of nanofluid over a convectively heated nonlinear stretching surface. *Int J Heat Mass Transf.* (2016) **100**:566–72. doi: 10.1016/j.ijheatmasstransfer.2016.04.113

30. Goshayeshi HR, Safaei MR, Goodarzi M, Dahari M. Particle size and type effects on heat transfer enhancement of Ferro-nanofluids in a pulsating heat pipe. *Powder Technol.* (2016) **301**:1218–26. doi: 10.1016/j.powtec.2016.08.007

31. Eid MR, Alsaedi A, Muhammad T, Hayat T. Comprehensive analysis of heat transfer of gold-blood nanofluid (Sisko-model) with thermal radiation. *Results Phys.* (2017) **7**:4388–93. doi: 10.1016/j.rinp.2017.11.004

32. Hayat T, Muhammad T, Shehzad SA, Alsaedi A. An analytical solution for magnetohydrodynamic Oldroyd-B nanofluid flow induced by a stretching sheet with heat generation/absorption. *Int J Therm Sci.* (2017) **111**:274–88. doi: 10.1016/j.ijthermalsci.2016.08.009

33. Hayat T, Sajjad R, Muhammad T, Alsaedi A, Ellahi R. On MHD nonlinear stretching flow of Powell-Eyring nanomaterial. *Results Phys.* (2017) **7**:535–43. doi: 10.1016/j.rinp.2016.12.039

34. Bhatti MM, Zeeshan A, Ellahi R. Simultaneous effects of coagulation and variable magnetic field on peristaltically induced motion of Jeffrey nanofluid containing gyrotactic microorganism. *Microvasc Res.* (2017) **110**:32–42. doi: 10.1016/j.mvr.2016.11.007

35. Muhammad T, Alsaedi A, Shehzad SA, Hayat T. A revised model for Darcy-Forchheimer flow of Maxwell nanofluid subject to convective boundary condition. *Chinese J Phys.* (2017) **55**:963–76. doi: 10.1016/j.cjph.2017.03.006

36. Muhammad T, Alsaedi A, Hayat T, Shehzad SA. A revised model for Darcy-Forchheimer three-dimensional flow of nanofluid subject to convective boundary condition. *Results Phys.* (2017) **7**:2791–7. doi: 10.1016/j.rinp.2017.07.052

37. Muhammad T, Lu DC, Mahanthesh B, Eid MR, Ramzan M, Dar A. Significance of Darcy-Forchheimer porous medium in nanofluid through carbon nanotubes. *Commun Theor Phys.* (2018) **70**:361. doi: 10.1088/0253-6102/70/3/361

38. Hayat T, Hussain Z, Alsaedi A, Muhammad T. An optimal solution for magnetohydrodynamic nanofluid flow over a stretching surface with constant heat flux and zero nanoparticles flux. *Neural Comp. Appl.* (2018) **29**:1555–62. doi: 10.1007/s00521-016-2685-x

39. Shehzad N, Zeeshan A, Ellahi R, Rashidi S. Modelling study on internal energy loss due to entropy generation for non-Darcy Poiseuille flow of silver-water nanofluid: an application of purification. *Entropy.* (2018) **20**:851. doi: 10.3390/e20110851

40. Ellahi R, Zeeshan A, Shehzad N, Alamri SZ. Structural impact of kerosene-Al$_2$O$_3$ nanoliquid on MHD Poiseuille flow with variable thermal conductivity: application of cooling process. *J Mol Liquid.* (2018) **264**:607–15. doi: 10.1016/j.molliq.2018.05.103

41. Shehzad N, Zeeshan A, Ellahi R. Electroosmotic flow of MHD Power law Al$_2$O$_3$-PVC nanofluid in a horizontal channel: Couette-Poiseuille flow model. *Commun Theor Phys.* (2018) **69**:655–66. doi: 10.1088/0253-6102/69/6/655

42. Zeeshan A, Shehzad N, Abbas T, Ellahi R. Effects of radiative electro-magnetohydrodynamics diminishing internal energy of pressure-driven flow of titanium dioxide-water nanofluid due to entropy generation. *Entropy.* (2019) **21**:236. doi: 10.3390/e21030236

43. Mabood F, Ibrahim SM, Khan WA. Effect of melting and heat generation/absorption on Sisko nanofluid over a stretching surface with nonlinear radiation. *Phys Scripta.* (2019) **94**:065701. doi: 10.1088/1402-4896/ab1164

44. Zeeshan A, Ellahi R, Mabood F, Hussain F. Numerical study on bi-phase coupled stress fluid in the presence of Hafnium and metallic nanoparticles over an inclined plane. *Int J Numer Methods Heat Fluid Flow*. (2019) **29**:2854–69. doi: 10.1108/HFF-11-2018-0677

45. Naqvi SMRS, Muhammad T, Kim HM, Mahmood T, Saeed A, Khan BS. Numerical treatment for Darcy-Forchheimer flow of nanofluid due to a rotating disk with slip effects. *Can J Phys*. (2019) **97**:856–63. doi: 10.1139/cjp-2018-0553

46. Turkyilmazoglu M. Direct contact melting due to a permeable rotating disk. *Phys Fluids*. (2019) **31**:023603. doi: 10.1063/1.5086724